

Yield and Fracture of Paper

(Angle of Initial Crack Propagation and Yield Zone Propagation)

Jong-Moon Park[†] and James L. Thorpe*

ABSTRACT

Traditional theories of the tensile failure of paper have assumed that uniform strain progresses throughout the sheet until an imperfection within the structure causes a catastrophic break. The resistance to tensile elongation is assumed to be elastic, at first, throughout the structure, followed by an overall plastic yield. However, linear image strain analysis (LISA) has demonstrated that the yield in tensile loading of paper is quite non-uniform throughout the structure. Traditional theories have failed to define the flaws that trigger catastrophic failure. It was assumed that a shive or perhaps a low basis weight area filled that role. Studies of the fracture mechanics of paper have typically utilized a well-defined flaw around which yield and failure could be examined. The flaw was a simple razor cut normal to the direction of tensile loading. Such testing is labeled mode I analysis. The included flaw in the paper was always normal to the tensile loading direction, never at another orientation. However, shives or low basis weight zones are likely to be at random angular orientations in the sheet. The effects of angular flaws within the tensile test were examined. The strain energy density theory and experimental work demonstrate the change in crack propagation from mode I to mode II as the initial flaw angle is changed from being normal to the direction of tensile loading. The initial angle of crack propagation as a function of the initial flaw angle is predicted and experimentally demonstrated.

1. Introduction

In the mid 1950's Rance¹⁾ summarized the status of knowledge regarding the load-elongation and subsequent failure behavior of paper. He stated, "from the earliest phase of elastic behavior, through the apparent phases of viscoelastic flow and plastic yield, through strain hardening to ultimate fracture ... the whole sequence is visualized as

elastic straining accompanied by progressive disruption of fiber to fiber bonds." Much of that reasoning prevails today. Paper was also recognized as a material filled with a multitude of inherent cracks and flaw where the crossing fibers formed bonds. The tensile loading of any material with flaws or imperfections was described by Griffith^{2,3)} in the early 1920's with his theory of crack propagation. The basic concept

• This research had been supported by Empire State Paper Research Institute, USA.

• School of Forest Resources, Chungbuk Nat'l Univ., Cheongju 361-763, Korea.

* College of Environmental Science & Forestry, State Univ. of New York, Syracuse, NY 13210, USA.

† Corresponding author: e-mail: jmpark@cbucc.chungbuk.ac.kr

of imperfection instability was that a crack will propagate when the elastic energy released by its growth is greater than the energy required to create fracture surfaces.

The work of Griffith was carried out on centered cracks with the tensile loading normal to the crack direction. With paper and many other materials the crack or flaw may not always be normal to the direction of loading. The initial crack may be random in inclination to the direction of loading in the fiber network within the paper. Also, with random crack orientation, shear as well as tensile failure will occur. Thus, with mixed mode I and mode II loading the crack may propagate in any direction depending on the orientation of the load and the initial crack position.

Crack propagation in the presence of tensile as well as shear loading was first studied by Erdogan and Sih^{4,5)} in the early 1960's. They presented theoretical and experimental results on initial crack propagation under combined plane tensile and transverse shear loading at both ends of a specimen with an initial center crack, as shown in Fig. 1. Both sliding and tearing modes of crack extension were taken into the fracture criteria for a range of initial crack angles. The theory was based on the strain energy density factor, *S*, which predicts the direction of crack growth under mixed mode conditions. The strain energy density theory^{6,7)} is most appropriate to the study of crack propagation in paper because of the random nature of the structure.

1. 1 Yield and fracture criteria

Today there are many tensile yield criteria available for paper and other structural materials. Most yield theories are derived from the assumption that yield occurs when stress, strain, or energy reaches a limiting

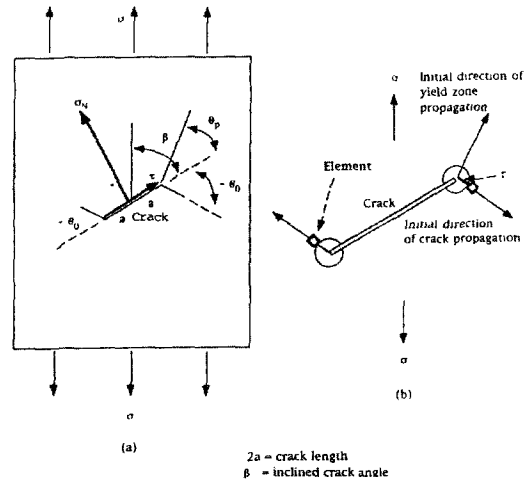


Fig. 1. Mixed mode fracture diagram.

value for homogeneous isotropic materials. The various types of yield theories are: (a) maximum principal stress theory [Lamé and Rankine]; (b) maximum shear stress theory [Guest,⁸⁾ Coulomb,⁹⁾ and Tresca¹⁰⁾]; (c) maximum strain theory [Saint-Venant¹¹⁾]; (d) maximum strain energy theory [Beltrami¹²⁾ and Haigh¹³⁾]; and (e) maximum shear energy theory [Huber,¹⁴⁾ Henky,¹⁵⁾ and von Mises¹⁶⁾]. Among these yield criteria, von Mises' is widely accepted, because it has been shown to be in excellent agreement with experiments for many ductile metals.¹⁷⁾ Von Mises' yield criterion can be described as

$$(\sigma_1 - \sigma_2)^2 + (\sigma_2 - \sigma_3)^2 + (\sigma_3 - \sigma_1)^2 = 2\sigma^2 \quad [1]$$

where $\sigma_1, \sigma_2, \sigma_3$ are the principal stress components. The equivalent stress, σ , is numerically equal to the tensile yield stress, σ_y .

Present day fracture criteria have been developed to follow the various yield criteria which can be applied to a material having flaws or cracks. Representative among the fracture criteria are (a) the strain energy release rate theory,^{2,3)} (b) the maximum

stress theory,⁴⁾ and (c) the strain energy density theory^{6,7)}.

Griffith's strain energy release rate theory is the classical concept in fracture mechanics. It is based on the global energy balance for a segment with crack extensions. It states that the crack propagates in the direction in which the energy release rate is a maximum and the initiation of failure occurs when the value of this release rate reaches a critical value. According to the Griffith theory, failure or crack propagation is normal to the direction of loading for a typical mode I tensile loading condition.

The maximum stress theory states that initial failure or crack propagation will grow in the direction perpendicular to the maximum stress. The maximum stress theory gives the same results as the strain energy release rate theory, since the direction in which the maximum circumferential stress occurs is also the direction causing the maximum energy release rate.⁴⁾

Griffith's theory has a limitation of application for mixed mode I and mode II loading conditions, because it assumes that the crack propagates by direct extension, in the manner shown in Fig. 2. a. In the pure tensile loading condition of mode I fracture, the crack grows in the expected manner. In the mixed mode loading condition of mode I and mode II, tension and shear forces are applied to the specimen and the crack grows in a non-similar manner (Fig. 2. b). Therefore, the stress intensity k_2 , which is related to skew-symmetric loading under in-plane shear, cannot be explained by the strain energy release rate theory.⁷⁾ This is a severe limitation because skew-symmetric loading is widely observed in multi-phased materials such as paper.

In Griffith's theory, the energy release rate of Mode II, G_2 , is computed by $G_2 = \pi k_2^2/E$ where k_2 and E are the stress intensity factors of mode II and Young's modulus,

respectively. However, k_2 is not valid since the crack does not propagate straight ahead, an assumption in Griffith's theory for Mode II as well as Mode I. Therefore, in mixed mode loading, simple addition of G_1 and G_2 for the crack energy release rate calculation is not applicable.⁷⁾ Application of Griffith's theory is limited to the Mode I loading condition which is a special case of mixed mode loading in which k_2 is zero.

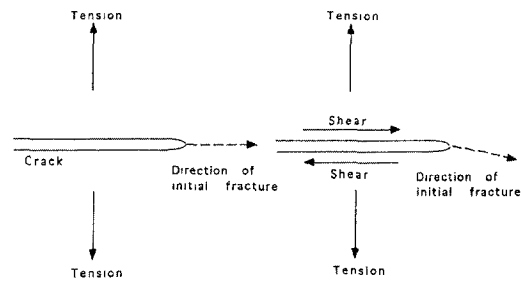


Fig. 2. Crack growth in (a) mode I loading and (b) mixed mode I and mode II loading.

1. 1. 1 Strain energy density theory^{6,7)}

When the strain energy, dW , is stored in an element volume dA , the strain energy density, dW/dA , stored in an element near the crack tip can be expressed as follows for a two-dimensional, homogeneous elastic stress system;

$$dW/dA = (1/r) (a_{11}k_1^2 + 2a_{12}k_1k_2 + a_{22}k_2^2) + \dots [2]$$

where r and θ are the distance and the angle of an element from the crack tip, respectively. The stress intensity factors k_1 and k_2 correspond to the mode I and II loading, respectively. They are different from those K_1 and K_2 of ASTM (The American Society for Testing and Material) by the factor of $\sqrt{\pi}$, i.e., $\sqrt{\pi} k_i = K_i$ ($i = 1, 2$) in the convention of

the strain energy density theory. The stress intensity factor, K_i , describes all the crack tip stresses in front of the crack tip. Fracture behavior of a material can be characterized by the stress intensity factor. Fracture occurs when the stress intensity factor exceeds a critical value, K_c . The critical value of the stress intensity factor, K_c , is regarded as a fracture toughness of a material. Linear elastic fracture mechanics (LEFM) is based on the stress intensity factor, K_i . The stress intensity factor, K_i , corresponds to J-integral for elastic plastic fracture mechanics (EPFM).

The coefficients a_{ij} ($i, j = 1, 2$) depend on the elastic constant κ and the shear modulus μ .

$$\begin{aligned}
 a_{11} &= \frac{1}{16\mu} [(1+\cos\theta)(\kappa - \cos\theta)] \\
 a_{12} &= \frac{1}{16\mu} \sin\theta[2\cos\theta - (\kappa - 1)] \\
 a_{22} &= \frac{1}{16\mu} [(\kappa+1)(1-\cos\theta)+(1+\cos\theta)(3\cos\theta-1)]
 \end{aligned}
 \tag{3}$$

where the elastic constant κ can be expressed by Poisson's ratio, γ , as $(3-4\gamma)$ for the plane strain case and $(3-\gamma)/(1+\gamma)$ for the plane stress case.

The magnitude of this energy density field is defined by the strain energy density factor, S , which is a value of strain energy density divided by the radius so it has the $1/r$ type singularity, as follows:

$$S = a_{11}k_1^2 + 2a_{12}k_1k_2 + a_{22}k_2^2
 \tag{4}$$

Details of the strain energy density theory are described in the following section.

1. 1. 2 Theoretical prediction of the initial angle of fracture and yield

(1) Direction of fracture initiation and propagation

The maximum stress theory assumes that the crack will start to propagate in the plane which is normal to the maximum circumferential stress, σ_θ . Therefore, the condition of the maximum theory, $\partial\sigma_\theta/\partial\theta = 0$, gives the following equation by obtaining derivative of tangential stress σ_θ with regard to θ :

$$k_1 \sin\theta_0 + k_2(3\cos\theta_0 - 1) = 0
 \tag{5}$$

where θ_0 is the initial angle of crack growth. In an inclined crack with length of $2a$ at an angle of β , with regard to the loading axis, as shown in Fig. 1, the stress intensity k_1 and k_2 have been described as follows⁵⁾:

$$\begin{aligned}
 k_1 &= \alpha\sqrt{a}\sin^2\beta \\
 k_2 &= \alpha\sqrt{a}\sin\beta\cos\beta
 \end{aligned}
 \tag{6}$$

When k_1 and k_2 are deleted by using equation [6], equation [5] becomes

$$\sin\theta_0 + (3\cos\theta_0 - 1) \cot\beta = 0, \beta \neq 0
 \tag{7}$$

Equation [7] states that the initial angle of crack growth, θ_0 , is only dependent on the inclined crack angle β , not on the elastic properties for an isotropic material.

On the other hand, the hypotheses of the strain energy density theory on crack initiation in a two-dimensional stress field are as follows:

(1) The initial crack growth takes place in the direction along which the strain energy density factor possesses a stationary minimum value, i.e.,

$$\partial S / \partial \theta = 0 \text{ at which } \theta = \theta_0
 \tag{8}$$

(2) Crack initiation occurs when the strain

energy density factor reaches a critical value, S_{cr} , i.e.,

$$a_{11}k_1^2 + 2a_{12}k_1k_2 + a_{22}k_2^2 = S_{cr} \text{ for } \theta = \theta_0 \quad [9]$$

where θ_0 is the angle of crack initiation and S_{cr} the critical strain energy density factor is regarded as a material constant. The strain energy density factor S is regarded as the resistance to fracture. Therefore, the crack propagates along the direction of the minimum resistance, e.g., the direction of the minimum value of S , S_{min} .¹⁸⁾

The strain energy density theory's condition $\partial S / \partial \theta = 0$ gives

$$\partial S / \partial \theta = (\kappa - 1) \sin(\theta - 2\beta) - 2\sin[2(\theta_0 - \beta)] - \sin 2\theta_0 = 0, \beta \neq 0 \quad [10]$$

Equation [10] states that the initial crack growth angle, θ_0 , depends on the inclined crack angle β and also on the elastic constant κ of the material.

(2) Direction of yield initiation

The strain energy density theory predicts that the direction of the maximum of the strain energy density, S_{max} , coincides with that of the maximum permanent deformation which is corresponding to yield.

Theoretical conditions of yield can be summarized as follows:

$$\partial S / \partial \theta = 0 \text{ and } \partial^2 S / \partial \theta^2 < 0$$

From equation [10], the direction of yield initiation, θ_p , should satisfy the following equations:

$$\begin{aligned} \partial S / \partial \theta &= (\kappa - 1) \sin(\theta_p - 2\beta) - 2\sin[2(\theta_p - \beta)] - \sin 2\theta_p = 0 \text{ and} \\ \partial^2 S / \partial \theta^2 &= (\kappa - 1) \cos(\theta_p - 2\beta) - 4\cos[2(\theta_p - \beta)] - 2\cos 2\theta_p < 0 \end{aligned} \quad [11]$$

where the angle of yield initiation, θ_p , is con-

ventionally defined as the counter-clockwise angle from the direction of original inclined angle as positive as shown in Fig. 1. In Mode I loading, when $\beta = 90^\circ$, the angle of yield initiation, θ_p , can be calculated by the following equation.¹⁹⁾

$$\theta_p = \pm \cos^{-1}(1 - 2\gamma) \quad [12]$$

2. Materials and Methods

Commercial photocopy paper, kraft sack, and newsprint were used in this study. The dimensions of the test specimens were the same as reported in previous work.²⁰⁾ A 10mm length (= 2a) crack was cut at the center of a specimen to make a single center-notched (SCN) specimen (Fig. 1). The inclined crack angle β was varied at 15, 30, 45, 60, 75, or 90°. For strain profile analysis, linear image strain analysis (LISA) was used.²¹⁾ The image observation area was 280 by 400 pixels, broken into a 14 by 20 grid of 280 strain observation elements, each 2.53 mm wide by 1.92 mm high. The total size of the observation area was 35.4 mm wide and 38.4 mm high. The angle of yield propagation was observed in the strain profile as the area of 125% of failure strain. The angle of initial crack propagation was measured on the specimen after failure in an Instron model 4204. The loading rate was 10 mm/min as described in previous work.²²⁾

3. Results and Discussion

3.1 Results

3.1.1 Strain profiles and yield zone

Strain profiles in the loading direction and shear strain profiles are shown in Figs. 3 - 8. The strain, load condition, and the inclined

crack angle, β , are described above and below each figure. In the strain profile, areas of 2.0 - 3.0% are shown lightly shaded and those over 3.0% are shaded dark. In the shear strain profiles, total shear strain areas of 0.5 - 1.5% are shown lightly shaded and over 1.5% shaded dark. In Fig. 3, the strain profiles of kraft sack, photocopy paper, and newsprint just before failure are shown when the inclined crack angle, β , is 30°. Fig. 1. 3. a, c, and e are y-strain profiles of photocopy paper, kraft sack, and newsprint, respectively. Fig. 3. b, d, and f are shear strain profiles of photocopy paper, kraft sack, and newsprint, respectively.

In Fig. 3. a for photocopy paper at a load of 14.5 Kg_f and a strain of 0.67%, strain areas of 1.0 - 1.5% shown lightly shaded are widely spread in front of the crack tip. Strain areas of 1.5 - 2.0% continue on a diagonal. In the strain profile of kraft sack at a load of 36.5 Kg_f and 1.08% strain shown in Fig. 3. c, high strain areas of 2.0 - 2.5% area aligned diagonally with the inclined crack. There are several isolated high strain areas of above 2.0%. In newsprint, as shown in Fig. 3. e, the load is 12.7 Kg_f and the strain 0.71%. The areas of strain over 2.0% are rather narrow compared to Fig. 3. a and c.

The shapes of the strain regions above 3.0% in front of the crack tip are different for each paper grade. Areas of high strain of kraft sack and photocopy paper in Fig. 3. a and c propagate and bend down. The strain above 3.0% for newsprint in Fig. 3. e stays close to the crack tip instead of extending.

Shear strains in Fig. 3. b, d, and f show the difference in the three papers tested. Fig. 3. b, copy paper at 14.5 Kg_f and 0.67% strain, shows shear strains above 0.5% are limited to the vicinity of the crack. In Fig. 3. d, kraft sack at 36.5 Kg_f and 1.08% strain, the shear strains above 0.5% extend upward from the crack into much of the top half of the observation area. Fig. 3. f is newsprint at 12.7 Kg_f

and 0.71% strain. Again, the shear strains above 0.5% are quite close to the crack.

Sequential loading, strain profiles of photocopy paper with an inclined crack angle, β , of 15, 45, and 90°, respectively, are shown in Figs. 4, 5, and 6.

At the inclined crack angle, β , of 15°, the strain distributions are perpendicular to the direction of loading. Only when the loading condition approaches failure at 0.85% strain do the strains above 3.0% appear at the crack tips.

In Fig. 5, strain profiles of photocopy paper are shown at an inclined crack angle, β , of 45°. The strain area above 2.0% appears in Fig. 5. b in front of the crack tip at a loading condition of 0.47% strain, which is 65.3% of ultimate strain, and 9.5 Kg_f load, which is 64.0% of ultimate load. In front of the crack tip, strain above 3.0% starts to propagate at the loading condition shown in Fig. 5. c, where 0.58% strain is 80.6% of ultimate strain, and 13.4 Kg_f load is 90.0% of the ultimate load. The high strain area above 3.0% in front of the crack tip propagates more than that of the inclined crack angle of 15° shown in Fig. 4. c, which has loading conditions similar to those in Fig. 5. c.

Strain profiles at the inclined crack angle of 90° are shown in Fig. 6. At initial loading conditions shown in Fig. 6. a, the area of 2.0 - 2.5% strain starts to appear. The loading conditions are 0.08% strain, which is 12.9% of the ultimate strain, and 2.0 Kg_f load, which is 16.4% of the ultimate load. In Fig. 6. c, areas above 3.0% strain continue to grow at 0.49% strain, which is 79.0% of ultimate strain, and 10.4 Kg_f load, which is 84.9% of ultimate load. Strain distribution patterns shown in Fig. 6 are rather symmetrical with the direction of loading when the inclined crack angle, β , is 90°.

The strain profiles of photocopy paper at different inclined crack angles are shown in Fig. 7. The inclined crack angle, β , was incre-

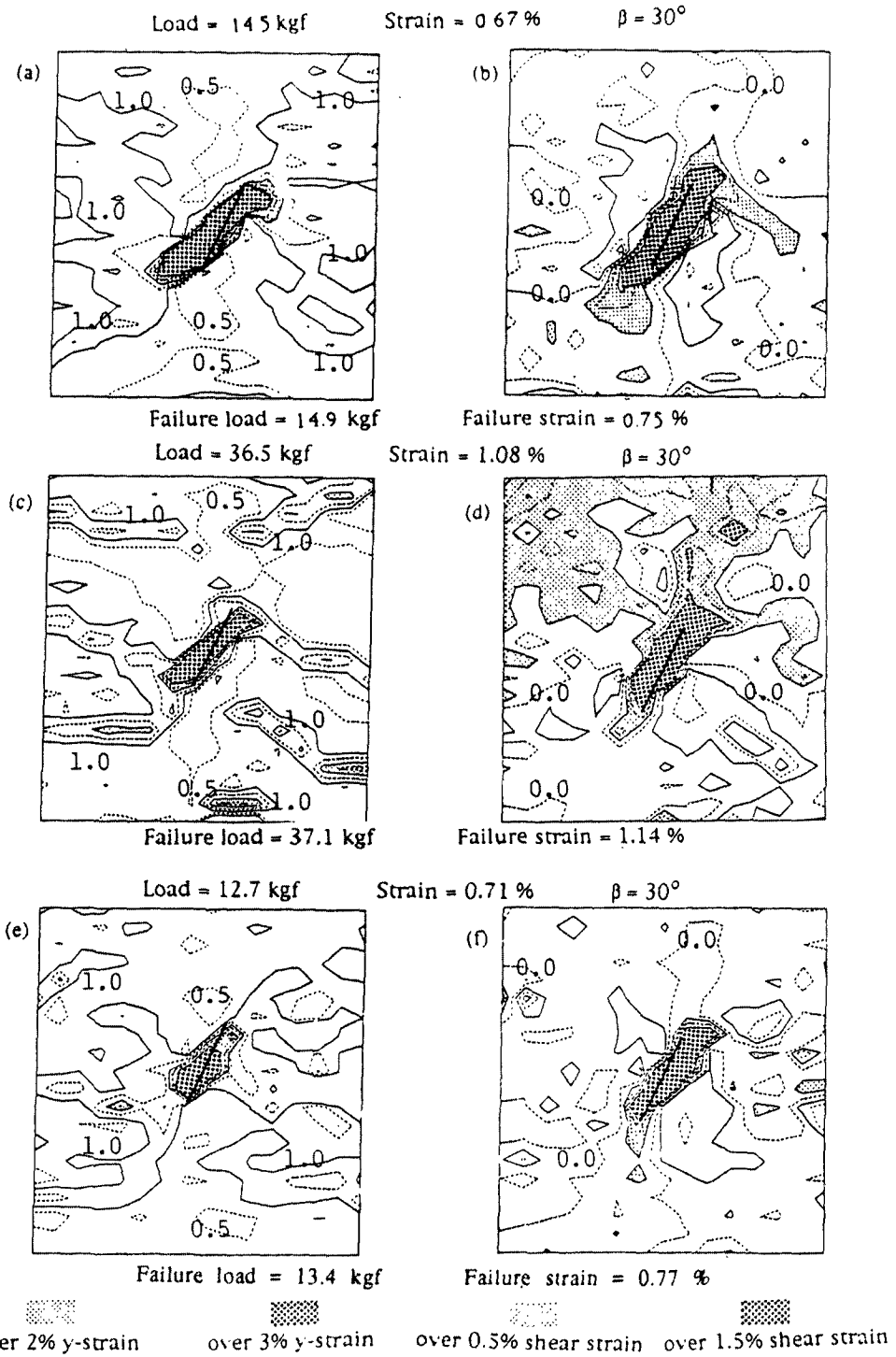
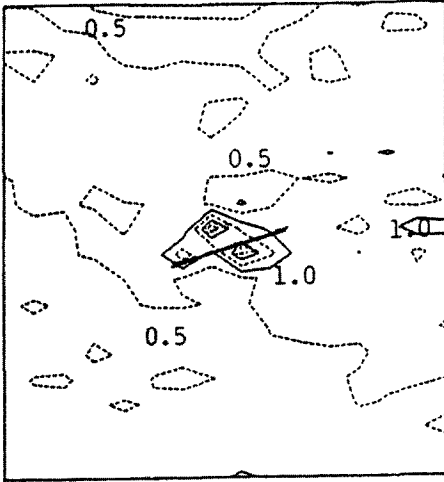
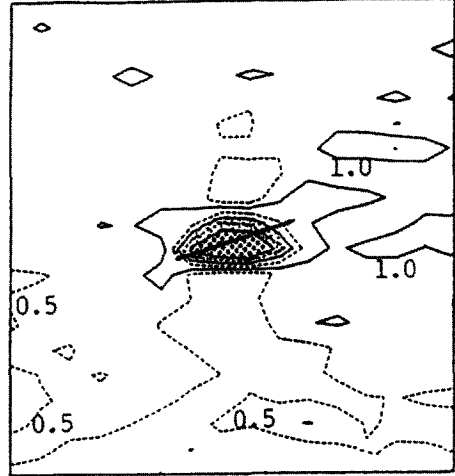


Fig. 3. Strain profiles in the loading direction and shear of photocopy paper, kraft sack, and newsprint at a crack angle, β , of 30° .

(a) Load = 10.4 kgf Strain = 0.45 %



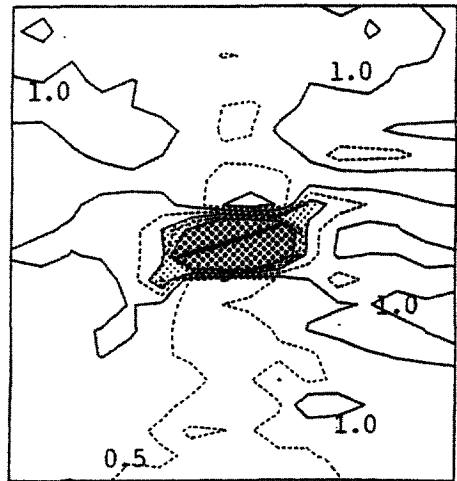
(b) Load = 13.6 kgf Strain = 0.64 %





(c) Load = 16.2 kgf Strain = 0.85 %



(d) Load = 17.1 kgf Strain = 0.95 %



 over 2% y-strain

 over 3% y-strain

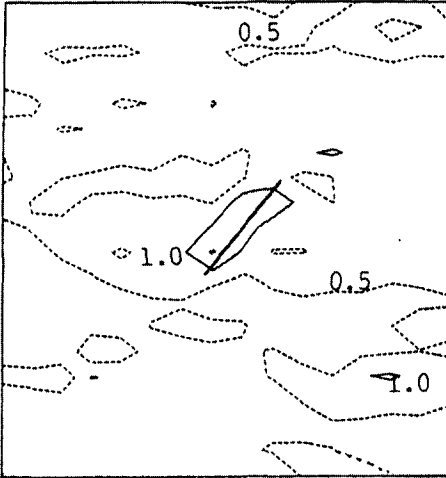
Failure load = 12.0 kgf

Failure strain = 0.62 %

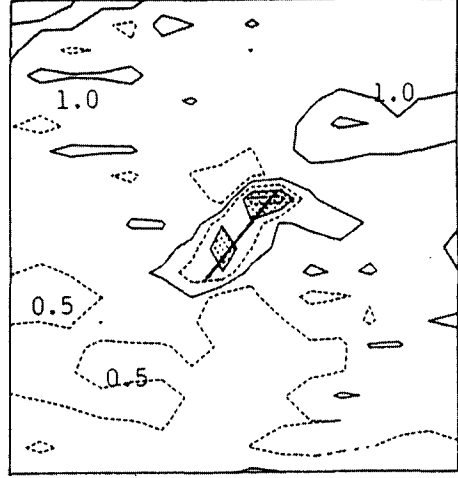
$\beta = 15^\circ$

Fig. 4. Strain profiles of photocopy paper in the loading direction at a crack angle, β , of 15° .

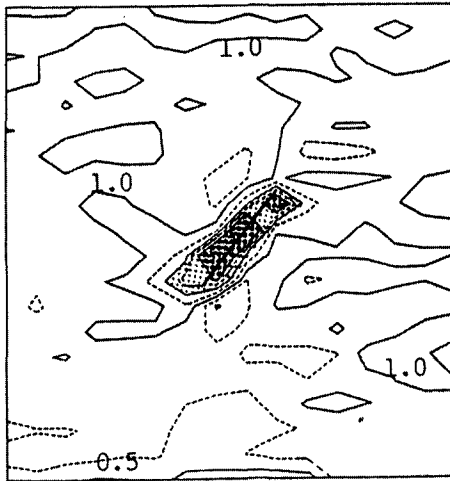
(a) Load = 4.2 kgf Strain = 0.17 %



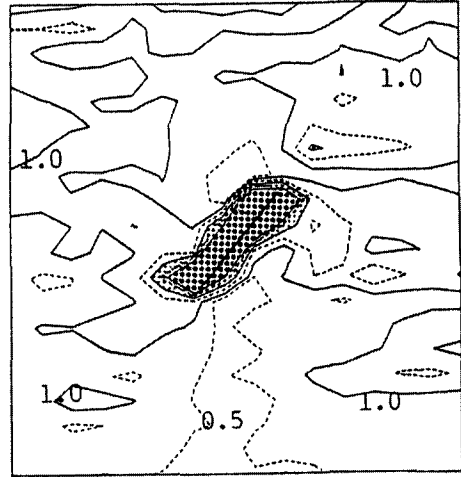
(b) Load = 9.5 kgf Strain = 0.47 %





(c) Load = 13.4 kgf Strain = 0.58 %



(d) Load = 14.6 kgf Strain = 0.68 %



 over 2% y-strain

 over 3% y-strain

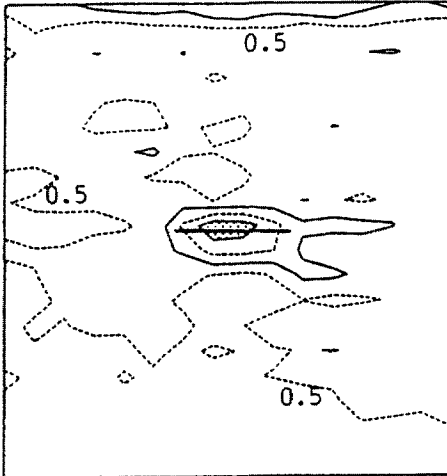
Failure load = 14.9 kgf

Failure strain = 0.72 %

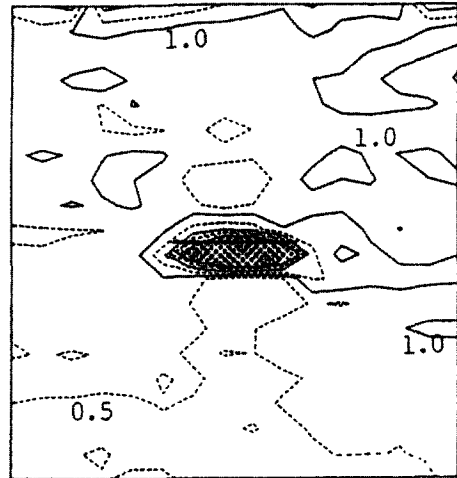
$\beta = 45^\circ$

Fig. 5. Strain profiles of photocopy paper in the loading direction at a crack angle, β , of 45° .

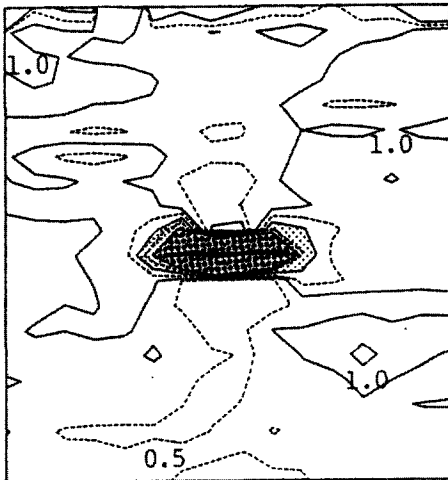
(a) Load = 2.0 kgf Strain = 0.08 %



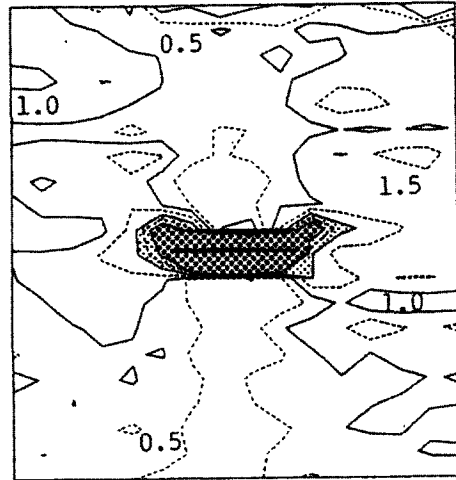
(b) Load = 6.4 kgf Strain = 0.28 %





(c) Load = 10.4 kgf Strain = 0.49 %



(d) Load = 11.8 kgf Strain = 0.60 %



 over 2% y-strain

 over 3% y-strain

Failure load = 12.2 kgf

Failure strain = 0.62 %

$\beta = 90^\circ$

Fig. 6. Strain profiles of photocopy paper in the loading direction at a crack angle, β , of 90° .

mented in six 15° increments from 15° to 90°. When the inclined crack angle, β , was 15°, the strain distribution was normal to the loading direction. Areas above 3.0% strain propagated from the crack tip as shown in Fig. 7. b - f, but not 7. a. The latter strain profile is similar to that of a specimen with no crack at the center. As the inclined crack angle, β , increased, the strain area above 2.0% strain propagated farther.

In Fig. 8, the shear strain profiles of photocopy paper are shown at progressively increasing inclined crack angle, β . The yield zone propagation was measured in the counterclockwise direction from the inclined initial cut.

The propagation angles of the yield zone predicted by the strain energy density theory are summarized in Table 1. It is difficult to assign a number to the propagation angle of yield zone, because the yield zone, in contrast to fracture propagation, does not approximate a line. Thus, the measured propagation angle of the yield zone is not included in Table 1, but it will be discussed in the discussion section.

3. 1. 2 The angle of fracture initiation

The angles of initial crack propagation were measured as the crack angle, β , was changed. Measured angles were compared with the angle predicted by the maximum stress theory and the strain energy density theory, and are summarized in Table 2.

Poisson's ratios are also included in the strain energy density theory for the plane stress case.

When the crack angle, β , equals zero, the problem becomes pure in-plane shear, mode II.

3. 2 Discussion

In previous work,²²⁾ it was shown that the angles of initial crack propagation and yield were different. That concept was surprising and perhaps contrary to traditional yield and failure concepts for paper. In pure mode I tensile loading, the propagation angle of the yield zone was roughly 60° whereas the angle of initial crack propagation direction was near 0°. The yield zone was conceived as a region that undergoes severe deformation beyond the yield point and the strain is high enough to permit bond rupture and fiber failure. On the other hand, the crack propagation is an extension of the fracture zone to complete failure. It is believed that quantitative differentiation of the yield and fracture is essential for understanding both mechanisms. The propagation direction of the yield zone and the fracture initiation were observed in the strain profiles and compared with those of theory.

3. 2. 1 Strain profiles and yield zone

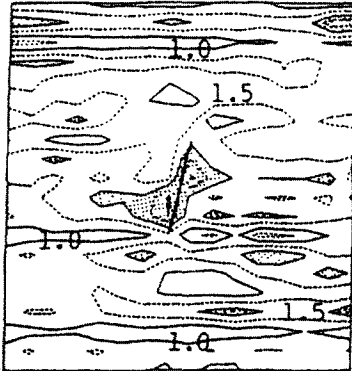
Strain profiles of photocopy paper, kraft sack, and newsprint were observed as the

Table 1. The predicted angle of yield zone propagation, θ_p , as a function of crack angle, β

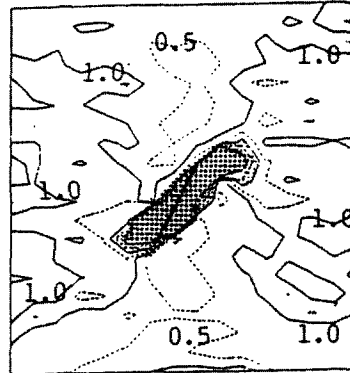
Crack Angle, β , °		15	30	45	60	75	90
θ_p , ° (Strain energy density theory)	$\gamma^a =$						
	0.0	0.0	0.0	0.0	0.0	0.0	0.0
	0.3	5.7	11.6	18.1	25.8	36.6	66.4
	0.5	7.5	15.3	23.8	33.7	47.3	90.0

^a γ =Poisson's ratio.

(a) Load = 17.1 kgf Strain = 0.95 % $\beta = 15^\circ$ (b) Load = 14.5 kgf Strain = 0.67 % $\beta = 30^\circ$

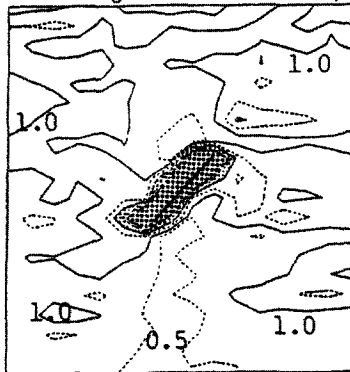


Fail load = 17.8 kgf Fail strain = 1.04 %

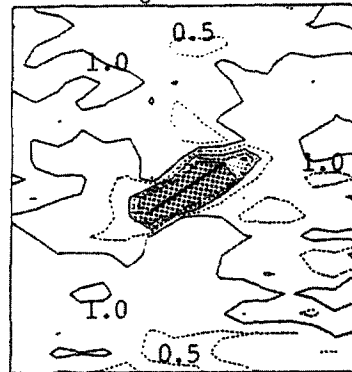


Fail load = 14.9 kgf Fail strain = 0.75 %

(c) Load = 14.6 kgf Strain = 0.68 % $\beta = 45^\circ$ (d) Load = 11.6 kgf Strain = 0.56 % $\beta = 60^\circ$

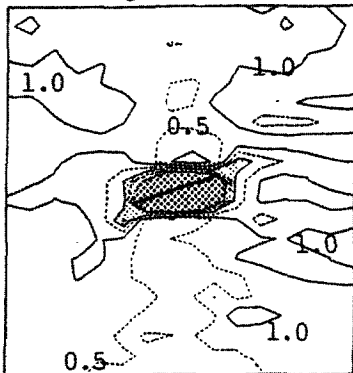


Fail load = 14.9 kgf Fail strain = 0.72 %

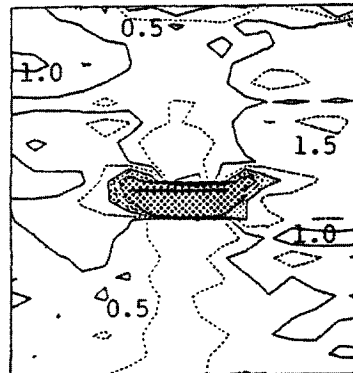


Fail load = 12.9 kgf Fail strain = 0.78 %


(e) Load = 11.5 kgf Strain = 0.51 % $\beta = 75^\circ$ (f) Load = 11.8 kgf Strain = 0.60 % $\beta = 90^\circ$



Fail load = 12.0 kgf Fail strain = 0.62 %



Fail load = 12.2 kgf Fail strain = 0.62 %

 over 2% y-strain


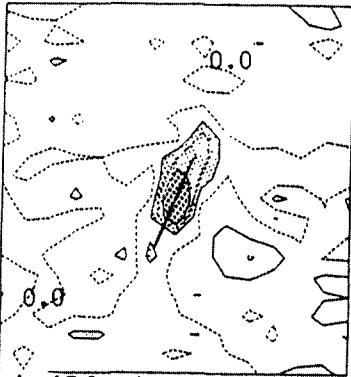
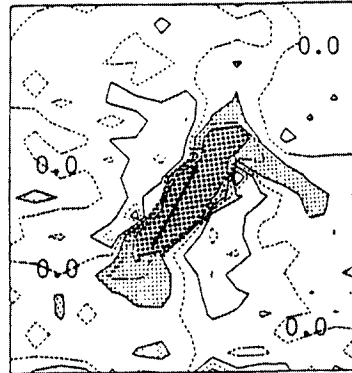
 over 3% y-strain

Fig. 7. Strain profiles of photocopy paper at progressively increasing crack angle, β .

(a) Load = 17.1 kgf Strain = 0.95 % $\beta = 15^\circ$ (b) Load = 14.5 kgf Strain = 0.67 % $\beta = 30^\circ$

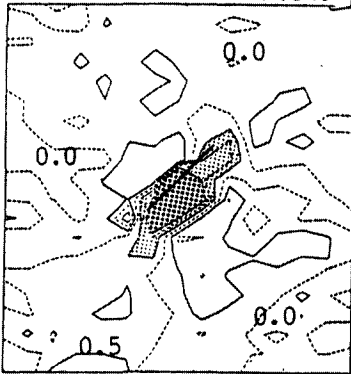


Fail load = 17.8 kgf Fail strain = 1.04 %



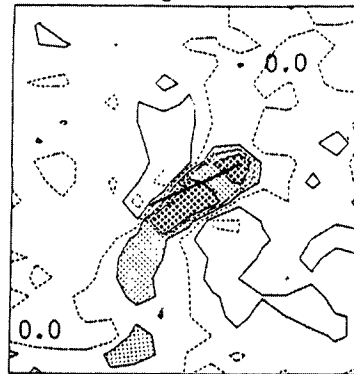
Fail load = 14.9 kgf Fail strain = 0.75 %

(c) Load = 14.6 kgf Strain = 0.68 % $\beta = 45^\circ$



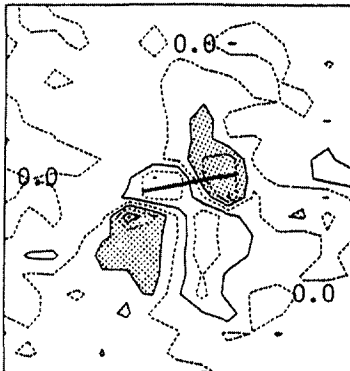
Fail load = 14.9 kgf Fail strain = 0.72 %

(d) Load = 11.6 kgf Strain = 0.56 % $\beta = 60^\circ$



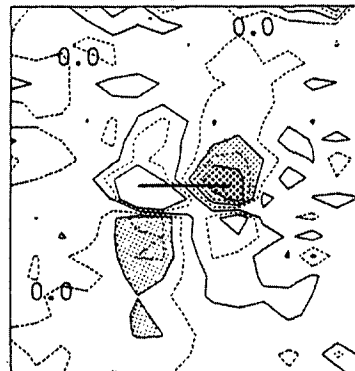
Fail load = 12.9 kgf Fail strain = 0.78 %

(e) Load = 11.5 kgf Strain = 0.51 % $\beta = 75^\circ$




Fail load = 12.0 kgf Fail strain = 0.62 %

(f) Load = 11.8 kgf Strain = 0.60 % $\beta = 90^\circ$



Fail load = 12.2 kgf Fail strain = 0.62 %

 over 0.5% shear strain


 over 1.5% shear strain

Fig. 8. Shear strain profiles of photocopy paper in the loading direction at different crack angles, β .

angle of the crack, β , was changed. When β was small, the paper hardly recognized the existence of the crack in all three paper grades. Strain values around the crack were only slightly higher than those of the surrounding areas.

The yield zone is closely related to the shear strain profiles shown in Figs. 3 and 8. The yield zone of the three different paper grades was roughly 90° counterclockwise from the fracture direction. As β , increased, the propagation angle of the yield zone, θ_p , also increased (Figs. 3 and 8).

In Fig. 3, it can be seen that the regions of strain above 3% just in front of the crack tip bend and propagate away from the direction of the original induced crack. The extent of bending and propagation of the high strain area in kraft sack paper is more significant than those of photocopy paper. The bending and strain propagation in newsprint is negligible. The bending may be related to a stress concentration phenomenon. In weak paper grades, stress concen-

tration is severe in front of the crack tip. In tough paper grades like kraft sack, the extent of bending and propagating increases as the stress absorbing ability increases.

The yield zone is a wide zone of fracture propagation. Nevertheless, the measured angle of yield zone is similar to the predicted angle as observed in Figs. 3 - 8.

3. 2. 2 The angle of fracture initiation

The predicted and measured angles of initial fracture propagation are compared in Table 2 at different crack angles, β . The pure in-plane shear experiment with $\beta=20^\circ$ is difficult and so the crack angle, β , goes only to 15° .

As shown in Figs. 3 - 8, the initial angle of fracture propagation is not predicted with Griffith's theory when the loading condition is combined mode I and mode II. According to Griffith's theory the angle of crack propagation should be perpendicular to the applied load regardless of the direction of

Table 2. The dependence of the angle of fracture initiation, θ_0 , on the crack angle, β , for the plane stress case

Crack Angle, β , $^\circ$		0	15	30	45	60	75	90
θ_0 , $^\circ$ (Maximum stress theory)		-	65.5	60.0	53.1	43.2	26.7	0
	$\gamma^a=$							
θ_0 , $^\circ$ (Strain energy density theory)	0.0	70.5	58.2	46.3	34.6	23.0	11.4	0
	0.1	74.2	62.9	52.1	41.7	31.7	20.8	0
	0.2	77.2	66.4	56.1	46.1	35.8	23.3	0
	0.3	79.7	69.2	59.1	49.1	38.4	24.5	0
	0.4	81.8	71.6	61.5	51.4	40.2	25.3	0
	0.5	83.6	73.5	63.5	53.1	41.5	25.8	0
θ_0 , $^\circ$ (Measured)								
	Kraft sack paper	-	76.1	63.1	61.0	50.0	23.4	0
		-	87.9	53.9	48.7	49.4	23.4	9.2
	Newsprint	-	-	63.3	43.0	25.7	19.2	16.5
		-	-	59.7	49.6	29.2	20.4	0
	Photocopy paper	-	76.4	59.9	55.4	38.1	20.5	5.7
	-	75.1	66.5	46.7	38.7	32.4	0	

^a γ =Poisson's ratio.

the induced crack.

To compare the measured angle of fracture propagation with the maximum stress theory and the strain energy density theory, predicted and measured angles of the initial crack propagation are presented in Fig. 9.

The predicted angle of the initial fracture propagation decreases as the induced crack angle increases. At a fixed induced crack angle, the angle of initial fracture propagation will increase as the Poisson's ratio increases. The maximum stress theory and the strain energy density theory agree when the induced crack angle is above 45°, but disagree when the induced crack angle is less than 45°. The measured initial angles of fracture propagation are shown in Fig. 9. As the crack angle increases, the measured angles of the initial fracture propagation decrease. Even though the measured angles of the initial fracture propagation are scattered, the observed angles of the initial fracture propagation display a trend similar to those of the maximum stress theory and the strain energy density theory. When the

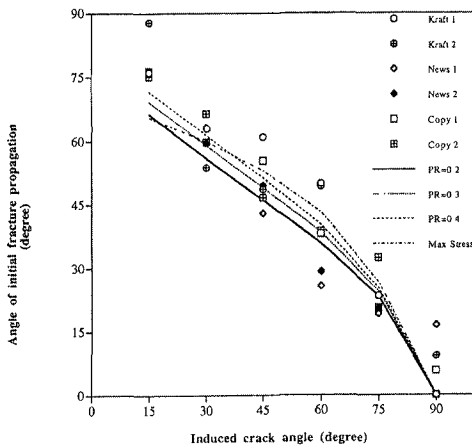


Fig. 9. The measured angle of initial fracture propagation.

*PR = Poisson's ratio, Max stress = Maximum stress theory, Kraft = Kraft sack paper, News = Newsprint, Copy = Photocopy paper.

induced crack angle is small, the measured angle of the crack propagation is closer to the strain energy density theory than the maximum stress theory. When the mode I loading condition prevails over mode II the strain energy density theory predicts the angles of the initial fracture propagation better than the maximum stress theory. The limited scatter in the data of the initial crack propagation as shown in Fig. 9 may be related to the expected differences in the three paper grades examined.

The critical stress intensities K_1 and K_2 are obtained and represented by Fig. 10 for photocopy paper, kraft sack, and newsprint.

According to the Griffith's theory, $K_1^2 + K_2^2 = K_{cr}^2$, where K_{cr} is a constant of a material. This means that K_1 and K_2 have a circular shape of the radius of $(K_1^2 + K_2^2)^{1/2}$ in K_1 and K_2 coordinates as shown in Fig. 10. In photocopy paper and newsprint, the stress intensity curve has a relatively constant radius when β is larger than 45°. As the inclined crack angle is less than 45°, the radius of stress intensity factor becomes smaller. Griffith's theory of initial crack propagation may be applied when β is larger than 45°. When β is greater than 45°, the ratio of K_2/K_1 is less than 1 and mode II failure is less than mode I failure. However, when the ratio of K_2/K_1 is greater than 1 and mode II failure predominates, the Griffith theory fails to predict failure correctly.

The radius of the stress intensity factor of tough paper grades like kraft sack paper also differs from the Griffith theory even when the mode I loading condition dominates. It is believed that kraft sack paper have elastic-plastic properties whereas Griffith's theory was derived for elastic material.

Under gradually increasing load, real failure modes in paper are very complex, they include fiber breakage as well as whole or partial debonding between fibers. Both ten-

sion and shear forces are applied to fibers and bonded areas that are randomly oriented to the applied load.

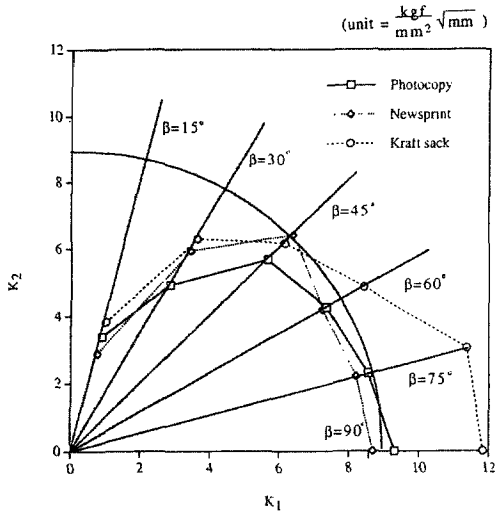


Fig. 10. The stress intensity factors K_1 and K_2 of photocopy paper, kraft sack, and newsprint.

4. Conclusions

As the initial crack angle is varied from normal to the direction of loading toward being in line with the tensile loading, crack propagation changes from predominantly mode I to mode II failure. Mode II failure is in-plane shear. Over a broad range of initial crack angles the strain energy density theory is more applicable to the analysis of crack propagation than Griffith's classic theory.

The strain energy density theory is applied successfully to paper to demonstrate that initial angle of crack propagation can be predicted.

Literature Cited

1. Rance, H. F., *Tappi*, 39(2):104-115 (1956).
2. Griffith, A. A., *The phenomena of rupture and flow in solids*, Philosophical Transaction, Royal Society of London, Series A 221, pp. 163-198 (1921).
3. Griffith, A. A., *The theory of rupture*, proceedings of First International Congress of Applied Mechanics, Benzene & Burgers (ed.), Walkman, 1925, pp. 55-63.
4. Erode, F., Shh, G. C., *J. Basic Eng.*, 85:519-527 (1974).
5. Sih, G. C., Paris, P. C., Erdogan, F., *Int. J. of Fracture Mech.*, 29:306-312 (1974).
6. Sih, G. C., *Int'l J. of Fracture*, 10(3):305-321 (1974).
7. Sih, G. C., *Mechanics of Fracture Initiation and Propagation*, Kluwer Academic Publishers, Dordrecht, 1991.
8. Guest, J. J. *Phil. Mag.* 50:69 (1900).
9. Coulomb, C. *A Mem. Math. et Phys.* 7:343 (1773).
10. Tresca, H., *Comptes Rendus Acad. Sci., Paris*, 59:754 (1864) & 64:809 (1867).
11. De Saint-Venant, *Comptes Rendus Acad. Sci. Paris*, 74:1009 & 1083 (1872).
12. Beltrami, E., *Rend. Ist. Lomb.* 18:704 (1885).
13. Haigh, B. P., *Brit. Ass. Reports, Section G* (1919).
14. Huber, M. T., *Czasopismo techniczne, Lemberg*, 22:81 (1904).
15. Henky, H. *Zeits. ang. Math. Mech.* 4:323 (1924).
16. Von Mises, R., *G ttinger Nachrichten, math-phys, Klasse*, 1913, pp. 582.
17. Hill, R., *Mathematical Theory of Plasticity*, Clarendon Press, 1967.
18. Xuefeng, W., Xinming, L., *Eng. Fract. Mechanics*, 34(1):55-64 (1989).
19. Sih, G. C., Faria, L. (eds), *Fracture Mechanics Methodology*, Martinus Nijhoff Publishers, The Hague, 1984.
20. Park, J. M., and Thorpe, J. L., *J. of Korea TAPPI*, 31(5):47 (1999).
21. Choi, D., Thorpe, J., Hanna, R., *Wood Sci. & Tech.*, 25:251 (1991).
22. Park, J. M. and Thorpe, J. L., *J. of Korea Tappi* 28(4):17-30 (1996).